Synthesis, Structure, and Magneto-transport of $LnNi_{1-x}Sb_2$ (Ln = Y, Gd−Er)

Evan Lyle Thomas,[†] Monica Moldovan,[‡] David P. Young,[‡] and Julia Y. Chan*[,†]

Department of Chemistry, Louisiana State University, 232 Choppin Hall, Baton Rouge, Louisiana 70803, and Department of Physics and Astronomy, Louisiana State University, Baton Rouge, Louisiana 70803

Received June 3, 2005. Revised Manuscript Received September 9, 2005

Single crystals of the ternary antimonides $LnNi_{1-x}Sb_2$ (Ln = Y, Gd−Er; $x \sim 0.4$) have been grown from antimony flux. X-ray diffraction experiments reveal that these compounds crystallize in the tetragonal space group *P4/nmm* (No. 129) with $Z = 2$. Lattice parameters are $a \sim 4.3$ Å and $c \sim 9.3$ Å. Adopting the $HfCuSi_2$ structure type, these compounds are layered and consist of Ln-capped Sb square nets and $NiSb_4$ tetrahedra arranged in an anti-PbO fashion. The $LnNi_{1-x}Sb_2$ compounds show antiferromagnetic ordering and field-dependent magnetization data are also presented. Transport measurements indicate metallic behavior and, most interestingly, positive magnetoresistance for each compound, with large positive magnetoresistance [$MR(\%) = (\rho_H - \rho_0)/\rho_0 \times 100$] above 100% for the Y-, Dy-, and Ho-analogues at 3 K and 9 T.

Introduction

Antimonides, particularly ternary lanthanide−transition metal−antimonides (Ln−T−Sb), are of interest due to their notable magnetic and transport properties and interesting structures.[1−4] The discovery of colossal magnetoresistance, up to −42% at 5 K and 5 T, in the Zintl phase $Eu_{14}MnSb_{11}$,[5] has led to study of magneto-transport behavior of Ln−T−Sb compounds.[1] At low temperatures, the hexagonal ZrBeSi-type compounds CeNiSb and NdNiSb also exhibit negative magnetoresistance (MR) behavior with values up to −13% at 2 K and 5 T and −18% at 22 K at 4 T, respectively.[6] Similarly, the magnetoresistance for $NdCrSb_3$[7] (orthorhombic $CeCrSb_3$-type) is negative up to −13% at 5 K and 4 T. Large negative magnetoresistance behavior at 2 K and fields between 4 and 5 T is observed in the LnNiSb compounds (cubic MgAgAs-type) with the heavier lanthanide elements Tb (−20%), Dy (−32%), and Ho (−27%).[6] In contrast, a few ternary antimonide compounds have been reported to exhibit small positive magnetoresistance behavior at temperatures below 5 K: nonmagnetic LuNiSb (cubic MgAgAs-type) with 1.5% at 8 T;[6] $Ce_3Rh_3Sb_4$ (cubic $Y_3Au_3Sb_4$-type) with ∼4% at 13 K and 4 T;[8] $LaCrSb_3$ ($CeCrSb_3$-type) with 5.5% at 150 K;[9] PrNiSb (hexagonal ZrBeSi-type) with 7% at 5 T;[6] and ∼10% at 4.5 T for the $HfCuSi_2$-type $LnCuSb_2$ (Ln = La, Ce) compounds.[10] However, $CeNiSb_2$ shows negative MR due to ferromagnetic ordering.[10] Furthermore, several antimonide phases display large positive magnetoresistance behavior, e.g., LaNiSb (ZrBeSi-type) up to 20% at 6.4 T,[6] and $Eu_{0.83}Fe_4Sb_{12}$ (cubic $LaFe_4P_{12}$-type) reaches a maximum at 130% at 2 K and 12 T.[11,12] Although the antimonides mentioned above do not comprise an exhaustive list, it becomes evident that the appearance of positive magnetoresistance, large in some cases, can be found and suggests that antimonides may yield interesting magnetic and transport behavior as well.

Magnetic and transport properties on polycrystalline samples of Kondo systems $CeTSb_2$ (T = Ni, Cu, Pd, and Ag) have been reported.[13] $CeCuSb_2$ and $CeAgSb_2$ order magnetically at 8 and 10 K, respectively. $CeTSb_2$ (T = Ni, Cu, and Au) have been shown to possess a quasi-two-dimensional electronic state from detailed studies of the electrical and magnetic properties on single crystals.[14,15] The $CeCuSb_2$ and $CeAuSb_2$ compounds are antiferromagnets with

* To whom correspondence should be addressed. E-mail: jchan@lsu.edu. Telephone: (225) 578-2695. Fax: (225) 578-3458.
[†] Department of Chemistry.
[‡] Department of Physics and Astronomy.

(1) Kauzlarich, S. M. *Chemistry, Structure and Bonding of Zintl Phases and Ions*; Series VCH Publishers: New York, 1996.
(2) Papoian, G. A.; Hoffmann, R. *Angew. Chem., Int. Ed.* **2000**, *39*, 2409−2448.
(3) Mills, A. M.; Lam, R.; Ferguson, M. J.; Deakin, L.; Mar, A. *Coord. Chem. Rev.* **2002**, *233*, 207−222.
(4) Sologub, O.; Salamakha, P. S. In *Rare Earth − Antimony Systems*; Gschneidner, K. A., Bünzli, J.-C. G., Pecharsky, V. K., Eds.; Elsevier: The Netherlands, 2003; Vol. 33, pp 35−146.
(5) Chan, J. Y.; Kauzlarich, S. M.; Klavins, P.; Shelton, R. N.; Webb, D. J. *Chem. Mater.* **1997**, *9*, 3132.
(6) Karla, I.; Pierre, J.; Skolozdra, R. V. *J. Alloys Compd.* **1998**, *265*, 42−48.
(7) Deakin, L.; Ferguson, M. J.; Mar, A.; Greedan, J. E.; Wills, A. S. *Chem. Mater.* **2001**, *13*, 1407−1412.
(8) Patil, S.; Paulose, P. L.; Gupta, L. C. *Solid State Commun.* **1999**, *109*, 217−222.
(9) Leonard, M. L.; Dubenko, I. S.; Ali, N. *J. Alloys Compd.* **2000**, *303*, 265−269.
(10) Lakshmi, K. V.; Menon, L.; Nigam, A. K.; Das, A.; Malik, S. K. *Physica B* **1996**, *224*, 289−291.
(11) Bauer, E.; Berger, S.; Galatanu, A.; Galli, M.; Michor, H.; Hilscher, G.; Paul, C.; Ni, B.; Abd-Elmeguid, M. M.; Tran, V. H.; Grytsiv, A.; Rogl, P. *Phys. Rev. B* **2001**, *6322*, art. no.-224414.
(12) Bauer, E.; Berger, S.; Galatanu, A.; Michor, H.; Paul, C.; Hilscher, G.; Tran, V. H.; Grytsiv, A.; Rogl, P. *J. Magn. Magn. Mater.* **2001**, *226*, 674−676.
(13) Muro, Y.; Takeda, N.; Ishikawa, M. *J. Alloys Compd.* **1997**, *257*, 23−29.
(14) Thamizhavel, A.; Takeuchi, T.; Okubo, T.; Yamada, M.; Asai, R.; Kirita, S.; Galatanu, A.; Yamamoto, E.; Ebihara, T.; Inada, Y.; Settai, R.; Onuki, Y. *Phys. Rev. B* **2003**, *68*, 054427.
(15) Thamizhavel, A.; Okubo, T.; Yamada, M.; Galatanu, A.; Yamamoto, E.; Inada, Y.; Ebihara, T.; Onuki, Y. *Physica B* **2003**, *327*, 374−377.

10.1021/cm051196a CCC: $30.25 © 2005 American Chemical Society
Published on Web 10/22/2005

T_N = 6.9 and 5.0 K, respectively, and single crystals of $CeNiSb_2$ are reported to have a ferromagnetic transition at T_c = 6.0 K.[14, 15]

Similar to $CeNiSb_2$ is $CeNiSb_3$, which also has a T_c of 6.0 K.[16] In our effort to grow single crystals of the rare-earth analogues of $CeNiSb_3$,[17] we have obtained high-quality single crystals of $LnNi_{1-x}Sb_2$ (Ln = Gd−Ho) and two new compounds $YNi_{1-x}Sb_2$ and $ErNi_{1-x}Sb_2$, where $x \sim 0.4$. The La member shows temperature-independent paramagnetism; the Ce, Pr, and Nd members are antiferromagnetic; and the Sm member shows van Vleck paramagnetism. Measurements on powders of the Gd-, Tb-, Dy-, and Ho-analogues order antiferromagnetically below Néel temperatures of 9, 12, 10, and <4 K, respectively.[18] However, magnetic measurements on powders by Szytula et al. show the Dy- and Ho-analogues to have metamagnetic transitions below T_M = 8.2 and 6.6 K, respectively.[19]

The structures of the $LnNiSb_2$ (Ln = Ce−Nd, Sm, and Gd−Ho) compounds[18,20] were determined from X-ray powder diffraction studies and are reported to crystallize with the $ZrCuSi_2$-type or $HfCuSi_2$-type structure.[21] Their attempts to synthesize the Y- and Er-analogues by arc-melting in argon were unsuccessful.[18] The structure of the $LnNi_{1-x}Sb_2$ (Ln = Y, Gd−Er) compounds, which has been described in detail,[21] consists of layers of $NiSb_4$ tetrahedra and layers of Sb square nets which are capped by Ln atoms. This family of compounds is isostructural to other $LnTSb_2$ (T = Mn, Fe, Co, Cu, Zn, Pd, Ag, Cd, Au, or substituted with main group elements In or Sn) compounds where the T constituent is slightly off stoichiometry and written as $LnT_{1-x}Sb_2$.[18,22−28]

To the best of our knowledge, previous magnetic measurements of polycrystalline $LnNiSb_2$ (Ln = Gd−Ho) samples have been limited to magnetization.[18,19,29,30] Herein we report the synthesis, structure, magnetization, electrical resistivity, and magnetoresistance behavior of $LnNi_{1-x}Sb_2$ (Ln = Y, Gd−Er) single crystals, and three new analogues (Ln = Y, Dy, Ho) of the family of antimonides with uncharacteristic large positive magnetoresistances.

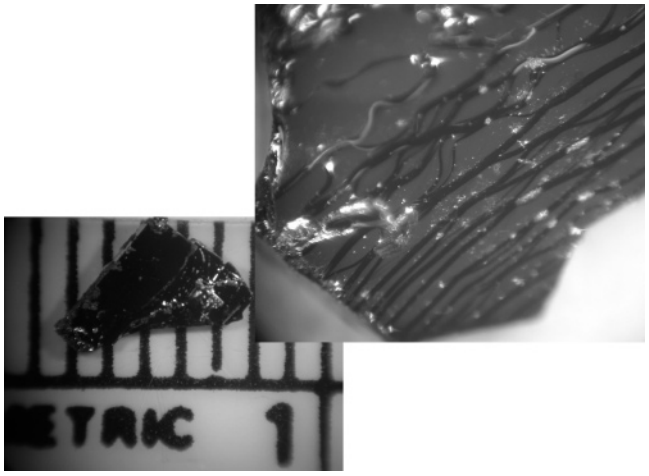

Figure 1. Shown is an aggregate of black $GdNi_{1-x}Sb_2$ single crystals. The blowup at the right highlights the layering along the *c*-axis within the crystal structure.

Experimental Section

Synthesis. The elements Y, Gd−Er (99.9%, ingot), Ni (99.999%, powder), and Sb (99.9999%, shot) were purchased from Alfa Aesar. Sample preparation was carried out in air as the ingots were cut into pieces, while the powder and shot were used as received and weighed. Single crystals of $LnNi_{1-x}Sb_2$ (Ln = Y, Gd−Er) were obtained by employing a flux-growth method using excess Sb. A 1:2:20 (Ln:Ni:Sb) molar ratio of the elements were combined in an alumina crucible. All samples, with a total mass of nearly 3.3 g, were covered with quartz wool and enclosed in fused silica tubes of approximately 10 cm in length. They were then heated to 1423 K for 2 h and cooled to 943 K at a rate of 5 K h^{-1}. To separate the single crystals, excess Sb flux was immediately filtered through the quartz wool by centrifugation. Black, plate-shaped crystals of $LnNi_{1-x}Sb_2$ (Ln = Y, Gd−Er) with dimensions up to 2 × 2 × 1 mm^3 were extracted with no noticeable degradation as a result of exposure to air for extended periods. An aggregate of single-crystal $GdNi_{1-x}Sb_2$ with layered morphology is shown in Figure 1.

Our original aim was toward the synthesis of single-phase $LnNiSb_3$ (Ln = Pr−Nd, Sm, and Gd−Yb). Synthesis of the Ce-analogue has been described previously.[31] Via the aforementioned synthetic treatment, the early lanthanide elements (Pr, Nd, Sm)[17] formed compounds which adopt the $CeNiSb_3$ structure type,[31] while the mid-lanthanide elements (Gd−Er) yielded compounds isostructural to $HfCuSi_2$. For this reason yttrium was chosen as the nonmagnetic analogue because of its comparable ionic radius. However, we note that $PrNiSb_2$, $NdNiSb_2$, and $SmNiSb_2$ can be synthesized by arc-melting.[18]

In addition to multiple lattice determinations from single crystals, X-ray powder diffraction data were collected on several ground single crystals of each compound to confirm sample homogeneity. The diffraction patterns show peaks that correspond to those of the $HfCuSi_2$ structure type.[21] The diffraction pattern of the Y-analogue sample, however, also contains peaks that are indexable to YSb.[32] $LnNiSb_2$ does not form for the Tm and Yb samples under our reaction conditions. Instead, TmSb (cubic NaCl-type) and a two-phase mixture of NiSb (hexagonal NiAs-type) and $NiSb_2$ (orthorhombic FeS_2-type) are formed for the Tm and Yb samples, respectively.

(16) Bao, W.; Macaluso, R. T.; Lee, H. O.; Nakatsuji, S.; Fisk, Z.; Chan, J. Y. In preparation.
(17) Thomas, E. L.; Macaluso, R. T.; Lee, H.; Fisk, Z.; Chan, J. Y. *J. Solid State Chem.* **2004**, *177*, 4228−4236.
(18) Sologub, O.; Hiebl, K.; Rogl, P.; Noël, H.; Bodak, O. *J. Alloys Compd.* **1994**, *210*, 153−157.
(19) Szytula, A.; Zygmunt, A. *J. Alloys Compd.* **2000**, *299*, 24−26.
(20) Pankevich, Y. V.; Pecharsky, V. K.; Bodak, O. I. *Russ. Metall.* **1983**, *5*, 189−191.
(21) Andrukhiv, L. S.; Lisenko, L. O.; Yarmolyuk, Y. P.; Gladishevskii, E. I. *Dopov. Akad. Nauk Ukr. RSR, Ser. B* **1975**, 645−648.
(22) Cordier, G.; Schafer, H.; Woll, P. *Z. Naturforsch.* **1985**, *40b*, 1097−1099.
(23) Leithe-Jasper, A.; Rogl, P. *J. Alloys Compd.* **1994**, *204*, 13−16.
(24) Flandorfer, H.; Sologub, O.; Godart, C.; Hiebl, K.; Leithe-Jasper, A.; Rogl, P.; Noël, H. *Solid State Commun.* **1996**, *97*, 561−565.
(25) Wollesen, P.; Jeitschko, W.; Brylak, M.; Dietrich, L. *J. Alloys Compd.* **1996**, *245*, L5−L8.
(26) Ferguson, M. J.; Hushagen, R. W.; Mar, A. *Inorg. Chem.* **1996**, *35*, 4505−4512.
(27) Ferguson, M. J.; Ellenwood, R. E.; Mar, A. *Inorg. Chem.* **1999**, *38*, 4503−4509.
(28) Deakin, L.; Ferguson, M. J.; Sprague, M. J.; Mart, A.; Sharma, R. D.; Jones, C. H. W. *J. Solid State Chem.* **2002**, *164*, 292−300.
(29) André, G.; Bourée, F.; Olés, A.; Penc, B.; Sikora, W.; Szytula, A. *Physica B* **1997**, *234*, 650−651.
(30) André, G.; Bourée, F.; Olés, A.; Penc, B.; Sikora, W.; Szytula, A.; Zygmunt, A. *J. Alloys Compd.* **1997**, *255*, 31−42.
(31) Macaluso, R. T.; Wells, D. M.; Sykora, R. E.; Albrecht-Schmitt, T. E.; Mar, A.; Nakatsuji, S.; Lee, H.; Fisk, Z.; Chan, J. Y. *J. Solid State Chem.* **2004**, *177*, 293−298.
(32) Schmidt, F. A. *J Less-Common Met.* **1970**, *21*, 415−425.

Table 1. Structural Refinement Data for $LnNi_{1-x}Sb_2$ (Ln = Y, Gd−Er)

compound	Y	Gd	Tb	Dy	Ho	Er
space group	*P4/nmm*	*P4/nmm*	*P4/nmm*	*P4/nmm*	*P4/nmm*	*P4/nmm*
a (Å)	4.2890(3)	4.3096(9)	4.2910(7)	4.2840(5)	4.2790(6)	4.275(5)
c (Å)	9.2990(9)	9.3974(16)	9.3220(14)	9.2660(12)	9.2350(10)	9.200(11)
V (Å^3)	171.06(2)	174.53(6)	171.64(5)	170.06(4)	169.09(4)	168.1(3)
Z	2	2	2	2	2	2
dimensions (mm)						
(min)	0.075	0.025	0.050	0.050	0.050	0.025
(mid)	0.125	0.025	0.075	0.075	0.050	0.075
(max)	0.150	0.100	0.100	0.100	0.075	0.075
temperature (K)	298(2)	298(2)	298(2)	298(2)	298(2)	298(2)
crystal density (g/cm^3)	7.098	8.328	8.462	8.605	8.708	8.728
θ range (deg)	2.19−30.00	4.34−29.91	2.18−29.97	4.40−29.95	2.21−30.02	2.21−30.02
μ (mm $^{-1}$)	35.22	37.144	38.870	40.382	41.941	43.253
collected reflections	493	391	388	468	399	409
unique reflections	181	185	184	182	180	182
R_{int}	0.0293	0.0463	0.0449	0.0431	0.0342	0.0307
h	−6 → 6	−6 → 6	−6 → 6	−6 → 6	−6 → 6	−6 → 6
k	−4 → 4	−4 → 4	−4 → 4	−4 → 4	−4 → 4	−4 → 4
l	−13 → 12	−13 → 9	−13 → 9	−13 → 11	−13 → 11	−8 → 12
$\Delta\rho_{max}$ (e Å^{-3})	2.013	2.456	4.048	2.747	2.615	2.273
$\Delta\rho_{min}$ (e Å^{-3})	−1.225	−1.394	−3.735	−2.874	−2.674	−3.707
extinction coefficient	0.0048(12)	0.0048(16)	0.0056(19)	0.0059(18)	0.0125(17)	0.029(3)
$R(F)$for $F_o^2 > 2\sigma(F_o^2)$[a]	0.0255	0.0300	0.0377	0.0363	0.0319	0.0314
$R_w(F_o^2)$[b]	0.0509	0.0707	0.0952	0.0852	0.0719	0.0715

[a] $R(F) = \sum||F_o| - |F_c||/\sum|F_o|$. [b] $R_w(F_o^2) = [\sum[w(F_o^2 - F_c^2)^2]/\sum[w(F_o^2)^2]]^{1/2}$.

Elemental Analysis. Semiquantitative microprobe elemental analysis was performed on an aggregate of $GdNi_{1-x}Sb_2$ single crystals with an Hitachi S-3600N Variable Pressure Scanning Electron Microscope (VP-SEM) with integrated energy dispersive spectroscopy (EDS) capabilities. Data were acquired using an accelerating voltage of 20 kV and 50 s acquisition times. The aggregate analyzed resulted in atomic ratios of approximately 1:0.67:2 (Gd:Ni:Sb). These results are in good agreement with the atomic ratios of 1:0.63:2, as obtained from single-crystal X-ray diffraction structural refinements.

Single-Crystal X-ray Diffraction. For crystal structure determinations, fragments with dimensions of ∼0.08 × 0.05 × 0.10 mm^3 were chosen and glued onto glass fibers and mounted onto the goniometer of a Nonius Kappa CCD X-ray Diffractometer. Data were collected using graphite monochromatized Mo Kα (λ = 0.71073 Å) radiation at room temperature. Lattice parameters of the $LnNi_{1-x}Sb_2$ (Ln = Y, Gd−Er) compounds were determined from a 15° φ scan. Table 1 lists the crystallographic information and other data collection parameters.

After an appropriate space group, *P4/nmm* (No. 129, origin #2), was selected and the direct methods of SIR97[33] were employed, structural calculations and refinements for $GdNi_{1-x}Sb_2$ were done using the SHELXL97 package.[34] The preliminary model and subsequent data were refined using the atomic positions reported for $HfCuSi_2$,[21] and later served as an initial model to refine the remaining $LnNi_{1-x}Sb_2$ (Ln = Y, Tb−Er) compounds. The experimental intensity data were corrected for absorption, and along with the application of a weighting scheme, all atoms were refined as anisotropic. An extinction coefficient was determined from the least-squares cycles. The refinement initially yielded an $R[F^2 > 2\sigma(F^2)]$ of 0.0756 with a relatively large displacement parameter ∼0.0400 Å^2 for the Ni atom. This led to the refinement of the occupation of the Ni (2a) atom site. To further check for deviations from the ideal composition, the occupations of the Gd (2c), Sb1 (2c), and Sb2 (2b) atomic parameters were refined in separate sequences of least-squares cycles. The Ni occupancy parameter refined to ∼63%; however, the Gd and Sb occupancy parameters remained close to full occupancy (>98%); therefore, the ideal compositions were used in the final least-squares cycles which furthermore yielded well-behaved displacement parameters. The U_{eq} values for the Sb1 atom remains somewhat large; however, the formula $GdNi_{0.63}Sb_2$ as obtained from the above tasks is comparable to the EDS results.

Table 2 shows the atomic positions, Wyckoff symmetry, anisotropic displacement parameters, and occupation of atoms for $LnNi_{1-x}Sb_2$ (Ln = Y, Gd−Er). The interatomic distances for these compounds are listed in Table 3 for comparison of the isostructural phases. Additional crystallographic information and data collection parameters are provided as Supporting Information.

Physical Property Measurements. Magnetic properties were measured on aggregates of single crystals using a Quantum Design SQUID magnetometer. The temperature-dependent susceptibility data were measured with an applied field of 1000 G up to room temperature after being cooled to 2 K under zero magnetic field. Field-dependent magnetization data were also collected from zero field to 9 T at 2 K. The resistivity (down to 2 K) and magnetoresistance (at 3 K) data have been measured using a standard four-probe method with a Quantum Design Physical Property Measurement System (PPMS) at ambient pressure.

Results and Discussion

Crystal Structure. The $LnNi_{1-x}Sb_2$ (Ln = Y, Gd−Er) compounds crystallize with the $HfCuSi_2$ structure type in the tetragonal space group *P4/nmm* (No. 129) with $Z = 2$. The structure of $GdNi_{1-x}Sb_2$ is shown in Figure 2. It is composed of layers of Sb square nets that are capped by Gd atoms, and layers of $NiSb_4$ tetrahedra arranged in an anti-PbO fashion.[35,36] The Ln, Ni, Sb1, and Sb2 atoms occupy the 2c, 2a, 2c, and 2b positions, respectively.

A common unit in layered antimonide intermetallic compounds such as $LnSb_2$,[37] $LnT_{1-x}Sb_2$,[18,22,24,25,38−41] $LnSn_x$-

(33) Altomare, A.; Burla, M. C.; Camalli, M.; Cascarno, G. L.; Giacovazzo, A.; Guagliardi, A.; Moliterni, A. G. G.; Polidori, G.; Spagna, R. *J. Appl. Crystallogr.* **1999**, *32*, 115−119.
(34) Sheldrick, G. M. *SHELXL-97, Program for Refinement of Crystal Structures*; University of Göttingen: Göttingen, Germany, 1997.
(35) Grønvold, F.; Haraldsen, H.; Vihovde, J. *J. Acta Chem. Scand.* **1954**, *8*, 1927.
(36) Byström, A. *Ark. Kemi. Min. Geol.* **1945**, *20A*, No. 11.
(37) Wang, R.; Steinfink, H. *Inorg. Chem.* **1967**, *6*, 1685.
(38) Leithe-Jasper, A.; Rogl, P. *J. Alloys Compd.* **1994**, *203*, 133−136.

Table 2. Atomic Positions, Site Symmetry, and U_{eq} Values for LnNi$_{1-x}$Sb$_2$ (Ln = Y, Gd−Er)

atom	Wyckoff site	*x*	*y*	*z*	occupancy	U_{eq} (Å^2)[a]
			YNi$_{0.57}$Sb$_2$			
Y	*2c*	1/4	1/4	0.76259(14)	1.000	0.0127(3)
Ni	*2a*	3/4	1/4	0	0.567(8)	0.0140(10)
Sb1	*2c*	1/4	1/4	0.13030(11)	1.000	0.0194(3)
Sb2	*2b*	3/4	1/4	1/2	1.000	0.0125(3)
			GdNi$_{0.63}$Sb$_2$			
Gd	*2c*	1/4	1/4	0.76214(8)	1.000	0.0150(3)
Ni	*2a*	3/4	1/4	0	0.631(13)	0.0184(14)
Sb1	*2c*	1/4	1/4	0.12966(13)	1.000	0.0214(4)
Sb2	*2b*	3/4	1/4	1/2	1.000	0.0153(4)
			TbNi$_{0.60}$Sb$_2$			
Tb	*2c*	1/4	1/4	0.76224(11)	1.000	0.0101(4)
Ni	*2a*	3/4	1/4	0	0.596(12)	0.0120(16)
Sb1	*2c*	1/4	1/4	0.13057(16)	1.000	0.0168(5)
Sb2	*2b*	3/4	1/4	1/2	1.000	0.0102(5)
			DyNi$_{0.59}$Sb$_2$			
Dy	*2c*	1/4	1/4	0.76260(9)	1.000	0.0137(4)
Ni	*2a*	3/4	1/4	0	0.592(13)	0.0169(15)
Sb1	*2c*	1/4	1/4	0.13178(14)	1.000	0.0205(4)
Sb2	*2b*	3/4	1/4	1/2	1.000	0.0137(4)
			HoNi$_{0.60}$Sb$_2$			
Ho	*2c*	1/4	1/4	0.76286(8)	1.000	0.0105(3)
Ni	*2a*	3/4	1/4	0	0.597(10)	0.0139(13)
Sb1	*2c*	1/4	1/4	0.13225(13)	1.000	0.0173(4)
Sb2	*2b*	3/4	1/4	1/2	1.000	0.0105(4)
			ErNi$_{0.53}$Sb$_2$			
Er	*2c*	1/4	1/4	0.76315(9)	1.000	0.0079(4)
Ni	*2a*	3/4	1/4	0	0.530(10)	0.0063(13)
Sb1	*2c*	1/4	1/4	0.13311(15)	1.000	0.0150(5)
Sb2	*2b*	3/4	1/4	1/2	1.000	0.0074(4)

[a] U_{eq} is defined as one-third of the trace of the orthogonalized U_{ij} tensor.

Table 3. Selected Interatomic Distances (Å) in *Ln*Ni$_{1-x}$Sb$_2$ (*Ln* = Y, Gd − Er)

compound	Y	Gd	Tb	Dy	Ho	Er
Sb2−Sb2 (×4)	3.0328(2)	3.0476(6)	3.0342(5)	3.0292(4)	3.0257(4)	3.023(4)
Ln−Sb2 (×4)	3.2498(10)	3.2729(4)	3.2526(8)	3.2418(7)	3.2358(6)	3.230(3)
Ln−Sb1 (×4)	3.1922(5)	3.2128(8)	3.1945(8)	3.1834(6)	3.1770(6)	3.170(3)
Ln−Ni (×4)	3.0778(9)	3.1048(7)	3.0847(8)	3.0703(6)	3.0616(6)	3.052(3)
Ni−Sb1 (×4)	2.4631(5)	2.4756(7)	2.4667(8)	2.4656(7)	2.4636(7)	2.464(2)

Sb_2,[27] and LnTSb$_3$[31,42] are the formation of square or nearly square Sb nets. Within the perfectly Sb square nets of LnNi$_{1-x}$Sb$_2$ (Ln = Y, Gd−Er) are Sb2 atoms which are coordinated to 4 other Sb2 atoms separated by distances of 3.0328(2) Å (Y), 3.0476(6) Å (Gd), 3.0342(5) Å (Tb), 3.0292(4) Å (Dy), 3.0257(4) Å (Ho), and 3.023(4) Å (Er).

The Ln atoms are inserted between the Sb nets and the $NiSb_4$ tetrahedra. In the LnNi$_{1-x}$Sb$_2$ structure, the Ln atoms cap the Sb nets, adopting an environment that is similar to the orthorhombic $LnSb_2$ structure.[37] The Ln atoms in LnNi$_{1-x}$Sb$_2$ possess a distorted square antiprismatic geometry as they are coordinated to 8 Sb atoms (4 Sb2 atoms as the square base and 4 Sb1 atoms which form a second square). With the substitution of smaller Ln elements, the distance between the Ln atom and the Sb square nets decrease as a result of lanthanide contraction. These distances are 3.2498(10) Å (Y), 3.2729(4) Å (Gd), 3.2526(8) Å (Tb), 3.2418(7) Å (Dy), 3.2358(6) Å (Ho), and 3.230(3) Å (Er).

The Ni atoms are coordinated to 4 Sb1 atoms, forming tetrahedral slabs. Although the Ni−Sb distances in the $NiSb_4$ slabs are equivalent for GdNi$_{1-x}$Sb$_2$, the Sb−Ni−Sb angles are not equivalent, causing the tetrahedra to be somewhat distorted. The Sb−Ni−Sb angles are 104.02(2)° and 121.03(5)° for GdNi$_{1-x}$Sb$_2$. These values are essentially equal to those found in the Y- and Tb−Er compounds.

The Ni site in these LnNi$_{1-x}$Sb$_2$ compounds is not fully occupied (see Table 2). The highest Ni occupancy is observed for the Gd-analogue, while the lowest occupancy is found for the Er compound. Deficiencies in the T site have also

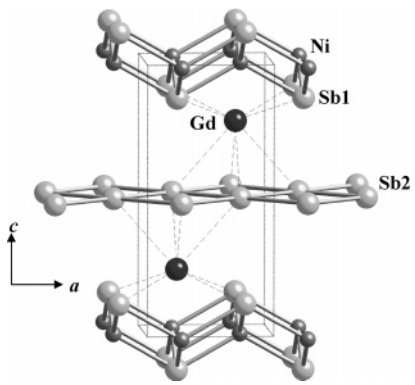

Figure 2. Shown is the structure of GdNi$_{1-x}$Sb$_2$ as viewed along the *bc*-plane with the unit cell outlined as a dotted line. The Gd atoms are represented as black circles, the Ni atoms are represented as heavily shaded circles, and the Sb atoms are the lightly shaded circles. Some bonds and atoms are not shown for clarity. The square antiprismatic environment of Gd is outlined by dashed lines.

(39) Brylak, M.; Möller, M. H.; Jeitschko, W. *J. Solid State Chem.* **1995**, *115*, 305−308.
(40) Sologub, O.; Noël, H.; Leithe-Jasper, A.; Rogl, P.; Bodak, O. I. *J. Solid State Chem.* **1995**, *115*, 441−446.
(41) Sologub, O.; Hiebl, K.; Rogl, P.; Bodak, O. I. *J. Alloys Compd.* **1995**, *227*, 40−43.
(42) Brylak, M.; Jeitschko, W. *Z. Naturforsch.* **1995**, *50b*, 899−904.

Table 4. Structural and Magnetic Data for $LnNiSb_2$ (Ln = Y, La−Nd, Sm, Gd−Er) Compounds[a] (Formulas Written with "Ideal" Stoichiometry)

formula	structure type[d]	ordering	ordering temperature T_c*, T_N (K)	θ (K)	μ_{exp} (μ_B)	μ_{calc} (μ_B)	reference
$YNiSb_2$	$HfCuSi_2$	PM[c]	NA[c]	NA	NA	0	this work
$LaNiSb_2$	$HfCuS_{i2}$	PM[b]	NA	NA	NA	0	18
$CeNiSb_2$	$HfCuSi_2$	AFM[b]	<4.0 K[b]	0.00	1.44	2.54	18
	$HfCuSi_2$	AFM[b]	3.5 K[b]	−39.2	2.50		24
	$HfCuSi_2$	FM[b]	*6.0 K[b]				8
	$HfCuSi_2$	FM[c]	*6.0 K[c]	−22.0	2.30−2.38		14
$PrNiSb_2$	"$HfCuSi_2$"	AFM[b]	6.0 K[b]	−4.00	4.00	3.58	18
	$CaBe_2Ge_2$[d]	AFM[b]	6.3 K[b]	−2.50	3.58		30
$NdNiSb_2$	"$HfCuSi_2$"	AFM[b]	<4.0 K[b]	−12.0	4.30	3.62	18
	$CaBe_2Ge_2$[d]	AFM[b]	2.3 K[b]	+6.00	3.70		30
$SmNiSb_2$	$HfCuSi_2$				1.80	0.85	18
$GdNiSb_2$	$HfCuSi_2$	AFM[b]	9.0 K[b]	−44.0	9.60	7.94	18
	$HfCuSi_2$	AFM[c]	4.2 K[c]	−60.0	9.12		this work
$TbNiSb_2$	"$HfCuSi_2$"	AFM[b]	12.0 K[b]	−44.0	10.80	9.72	18
	$CaBe_2Ge_2$[d]	AFM[b]	12.0 K[b]	−2.50	9.10		30
	$HfCuSi_2$	AFM[c]	5.6 K[c]	−29.0	9.69		this work
$DyNiSb_2$	$HfCuSi_2$	AFM[b]	10.0 K[b]	−27.0	13.00	10.65	18
	$HfCuSi_2$	AFM[b]	8.2 K[b]	−5.00	10.20		19
	$HfCuSi_2$	AFM[c]	2.9 K[c]	−14.0	10.00		this work
$HoNiSb_2$	$HfCuSi_2$	AFM[b]	<4.0 K[b]	−12.0	10.20	10.61	18
	$HfCuSi_2$	AFM[b]	6.6 K[b]	−4.50	9.80		19
	$HfCuSi_2$	AFM[c]	4.9 K[c]	−10.0	10.75		this work
$ErNiSb_2$	$HfCuSi_2$	AFM[c]	3.5 K[c]	−7.00	10.71	9.58	this work

[a] Abbreviations: AFM, antiferromagnetic; PM, paramagnetic; FM, ferromagnetic; T_c, Curie temperature; T_N, Néel temperature; μ_{exp}, experimental effective moment; μ_{calc}, calculated effective moment for Ln^{3+}. [b] Experimental data collected on polycrystalline samples. [c] Experimental data collected on single crystals. [d] Note that the structures of the $LnNiSb_2$ (Ln = Pr, Nd, Tb) compounds are defect structures of the $CaBe_2Ge_2$ structure type.[46]

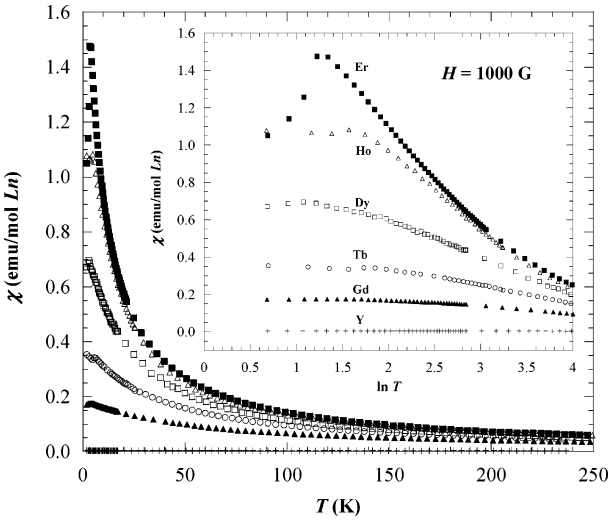

Figure 3. Zero field-cooled magnetic susceptibility (χ) as a function of temperature (T) with an applied field of $H = 1000$ G for single crystals of $LnNi_{1-x}Sb_2$ (Ln = Y, Gd−Er). The inset shows the ln(T) behavior.

been observed in the structurally related compounds CeT_xSb_2 (T = Mn, Fe, Co, Zn, Cu)[24] and $LaTSb_2$ (T = Mn, Co, Zn),[22] and also in the $LnIn_{1-x}Sb_2$[27] and $LnSn_xSb_2$ compounds.[26]

Physical Properties. The temperature-dependent magnetic susceptibility of the $LnNi_{1-x}Sb_2$ compounds follows a Curie−Weiss Law ($[\chi = C/(T - \theta)]$, where C is the Curie constant and θ is the Weiss temperature) down to 6 K in an applied field of 1000 G as shown in Figure 3. Susceptibility data were measured on single crystals. Weak temperature-dependent paramagnetic behavior is observed for the Y compound. At low temperatures (below 6 K), a kink in the susceptibilities of the Gd−Er-analogues can be observed. $DyNi_{1-x}Sb_2$ orders antiferromagnetically below 2.9 K, $ErNi_{1-x}Sb_2$ below 3.5 K, $GdNi_{1-x}Sb_2$ below 4.2 K, $HoNi_{1-x}Sb_2$ below 4.9 K, and $TbNi_{1-x}Sb_2$ below 5.6 K. These data vary greatly from the reported data, where measurements were performed on powder samples.[10,14,18,19,24,30] Table 4 compares the previously reported data for compounds in the $LnNiSb_2$ series. A linear fit was applied to the paramagnetic regions of each inverse susceptibility plot following the Curie−Weiss law $[1/\chi = (1/C)T - (\theta/C)]$ to obtain Weiss temperatures. The fits extrapolate to negative θ values ca. −60, −29, −14, −10, and −7 K for the Gd-, Tb-, Dy-, Ho-, and Er-analogues, respectively, which is indicative of antiferromagnetic interactions. Experimental effective moments obtained from the equation $\mu_{eff} = \sqrt{8C}$, for the $LnNi_{1-x}Sb_2$ compounds are 9.12 μ_B, 9.69 μ_B, 10.00 μ_B, 10.75 μ_B, and 10.71 μ_B for Ln = Gd, Tb, Dy, Ho, and Er, respectively. These values are close to the expected values for the Ln^{3+} free ions (Table 4). The experimental effective moments for the magnetic rare-earth ions in the Gd and Er compounds are slightly larger than the theoretical values obtained for these elements in the trivalent state. The nonmagnetic analogue $YNi_{1-x}Sb_2$ does not order magnetically and neither does the temperature-independent Pauli paramagnet $LaNiSb_2$,[18] suggesting that the magnetic behavior of the $LnNi_{1-x}Sb_2$ compounds is due solely to the magnetic rare-earth atoms, as supported by the experimental effective moments. The magnetic interaction, or long-range magnetic order of these compounds, can likely be described by the RKKY (Ruderman-Kittel-Kasuya-Yosida) theory due to the relatively large distances ~5.7 Å between the neighboring magnetic ions within the structures.

Figure 4 shows the field-dependent magnetization $M(H)$ at 2 K for single crystals of $LnNi_{1-x}Sb_2$ (Ln = Gd−Er). The magnetization of the Dy- and Ho-analogues begins to show signs of saturation below their theoretical saturation moments (μ_s) of 10 μ_B as calculated from the equation $\mu_s = gJ$, where g is the Landé factor and J is the total angular momentum of the Ln^{3+} ion. Below 3 T, a linear relationship of the

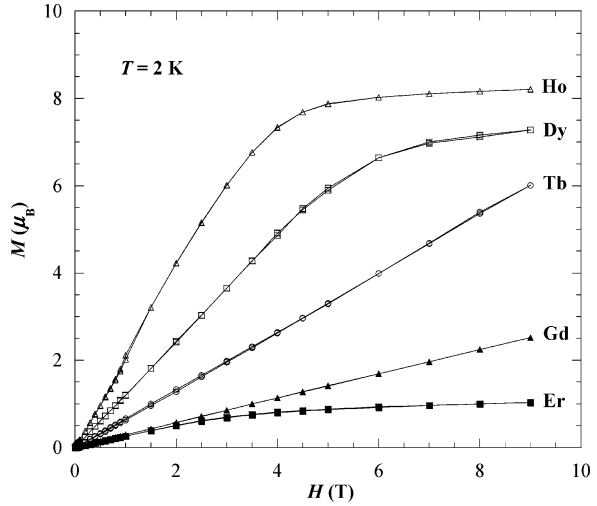

Figure 4. Field dependence (H) of the magnetization (M) of single crystals of $LnNi_{1-x}Sb_2$ (Ln = Gd−Er) at $T = 2$ K.

magnetization-to-field, typical for antiferromagnetically ordering compounds, is observed for each analogue with no hysteresis present. The Gd (theoretical $\mu_s = 7\ \mu_B$), and Tb compounds (theoretical $\mu_s = 9\ \mu_B$) show no signs of saturation up to 9 T.

A plot of the temperature-dependent electrical resistivity (ρ) of single crystals of $LnNi_{1-x}Sb_2$ (Ln = Y, Gd−Er) along the *ab*-plane is shown in Figure 5a,b. Each sample exhibits metallic character, with the Gd-analogue (Figure 5a) possessing the lowest resistivity ~20 $\mu\Omega$-cm at room temperature. Residual resistivity ratios (RRR = ρ_{298K}/ρ_{2K}) for these samples range from 1 to 4. There is a drop in the resistivity of the Dy- and Ho-analogues, a phenomenon commonly observed in rare-earth intermetallics and attributed to Kondo lattice behavior. The magnetoresistance, defined as MR(%) = $(\rho_H - \rho_0)/\rho_0 \times 100$, at 3 K and H parallel to the *c*-axis for each $LnNi_{1-x}Sb_2$ compound is shown in Figure 6. The magnetoresistance behavior for these antiferromagnetic samples is probably due to electron-spin scattering at low temperatures.[43] The MR of the Dy- and Ho-analogues begins to saturate near 5 T above 100% and 150%, respectively. No evidence of saturation for the Y- and Er-analogues is seen up to 9 T. Large magnetoresistance has been observed in other layered nonmagnetic antimonides, most notably in the rare-earth diantimonide $LaSb_2$ whose MR > 750% at $T = 2$ K and $H \parallel c$ at 5.5 T[44] and MR > 8500% at $T = 2$ K and $H \perp ab$-plane at 45 T.[45] Overall, the magnetoresistance behavior for these compounds is systematic and scales with the bulk magnetism and correlated to the magnetization.

Large positive magnetoresistance behavior at 9 T is observed for each compound in $LnNi_{1-x}Sb_2$ ($x \sim 0.4$). The Dy- and Ho-analogues possess MR values above 100%, while the MR for the Y and Er compounds continually increases with increasing field. Although the ordering

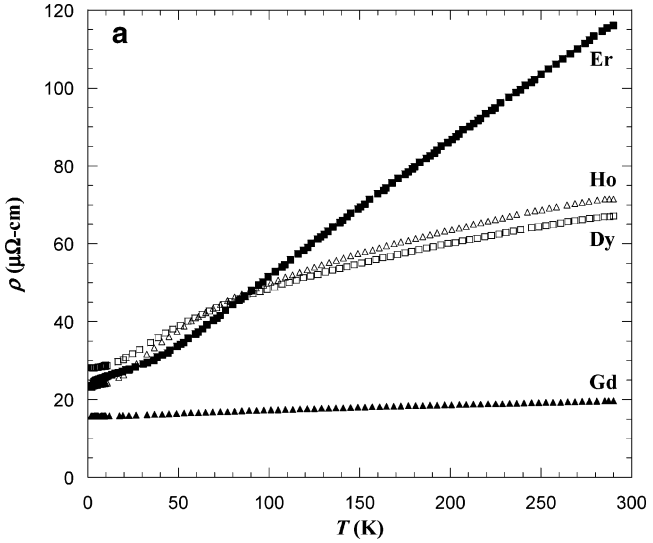

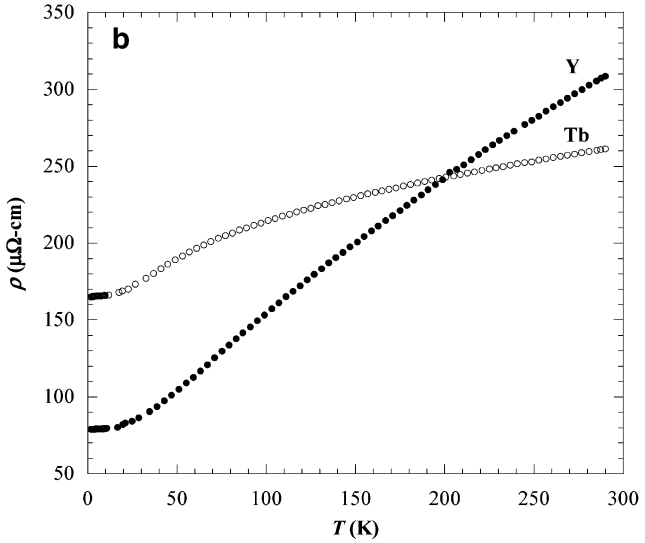

Figure 5. Temperature dependence (T) of the electrical resistivity (ρ) of single crystals of (a) Ln = Gd, Dy, Ho, Er and (b) Ln = Y, Tb down to 2 K along the *ab*-plane.

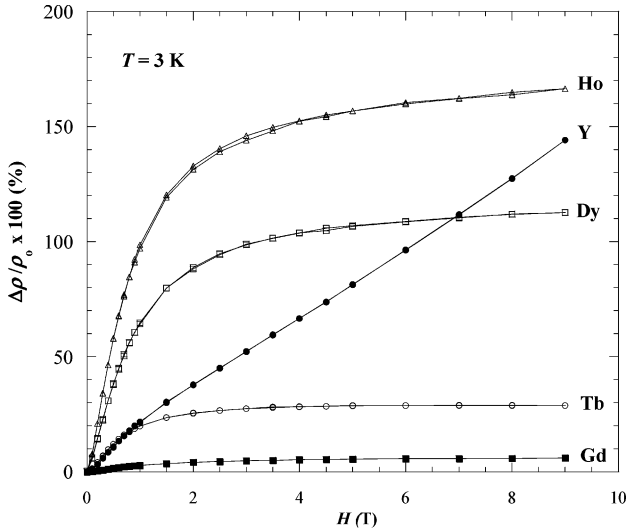

Figure 6. Field dependence of the magnetoresistance ($\Delta\rho/\rho_0 \times 100$) at $T = 3$ K measured on single crystals of $LnNi_{1-x}Sb_2$ (Ln = Y, Gd−Er) along the *ab*-plane with an applied field up to 9 T parallel to the *c*-axis.

temperatures of these compounds do not scale with the de Gennes factor [$dG = (g - 1)^2 J(J + 1)$], the magnetization

(43) Yamada, H.; Takada, S. *Prog. Theor. Phys.* **1973**, *49*, 1401−1419.
(44) Bud'ko, S. L.; Canfield, P. C.; Mielke, C. H.; Lacerda, A. H. *Phys. Rev. B* **1998**, *57*, 13624−13638.
(45) Young, D. P.; Goodrich, R. G.; Ditusa, J. F.; Guo, S.; Adams, P. W.; Chan, J. Y.; Hall, D. *Appl. Phys. Lett.* **2003**, *82*, 3713−3715.
(46) Hoffmann, W. K.; Jeitschko, W. *J. Less-Common Met.* **1988**, *138*, 313−322.

is due to the magnetic rare-earth ions and correlates systematically with the number of f-electrons.

It is worthwhile to note that these $LnNi_{1-x}Sb_2$ (Ln = Y, Gd−Er) compounds exhibit different ordering temperatures from the previously reported polycrystalline samples. This has also been the case for $CeNiSb_2$, where magnetic studies show an antiferromagnetic transition at $T_N < 4$ K;[18,24] however, magnetization experiments performed on single crystals show a ferromagnetic transition at $T_c = 6.0$ K.[10,14,15] The analysis of aggregates of single crystals of these $LnNi_{1-x}Sb_2$ (Ln = Y, Gd−Er) compounds eliminates some ambiguity of their magnetic property data and will allow for a correlation of their crystal chemistry and physical properties.

Acknowledgment. J.Y.C acknowledges the PRF-G, NSF Career (DMR 0237664), and Alfred P. Sloan Fellowship for partial support of this project.

Supporting Information Available: Additional information in CIF format. This material is available free of charge via the Internet at http://pubs.acs.org.

CM051196A